Experimental synthesis of chlorite from smectite at 300ºC in the presence of metallic Fe

D. Guillaume, A. Neaman, M. Cathelineau, Régine Mosser-Ruck, C. Peiffert, Mustapha Abdelmoula, J. Dubessy, F. Villieras, A. Baronnet, N. Michau

Clay Minerals (2003) **38**, 281–302

Experimental synthesis of chlorite from smectite at 300°C in the presence of metallic Fe

D. GUILLAUME[1,*,†], A. NEAMAN[2], M. CATHELINEAU[1], R. MOSSER-RUCK[1], C. PEIFFERT[1], M. ABDELMOULA[3], J. DUBESSY[1], F. VILLIÉRAS[2], A. BARONNET[4] AND N. MICHAU[5]

[1] Géologie et Gestion des Ressources Minérales et Energétiques (G2R), UMR 7566 CNRS-CREGU-INPL-UHP, Université Henri Poincaré, BP 239, 54506 Vandœuvre-lès-Nancy, [2] Laboratoire Environnement et Minéralurgie (LEM), UMR 7569 CNRS-INPL, Ecole Nationale Supérieure de Géologie, BP 40, 54501 Vandœuvre-lès-Nancy, [3] Laboratoire de Chimie Physique et Microbiologie pour l'Environnement (LCPME), UMR 7564 CNRS-UHP, Université Henri Poincaré, 405 rue de Vandœuvre, 54600 Villers-lès-Nancy, [4] Centre de Recherche sur les Mécanismes de Croissance Cristalline CRMC2-CNRS, Campus Luminy, case 913, 13288 Marseille, and [5] Agence nationale pour la gestion des déchets radioactifs (ANDRA), Direction Scientifique/Service Matériaux, Parc de la Croix Blanche, 1/7 rue Jean Monnet, 92298 Châtenay-Malabry, France

(*Received 28 January 2002; revised 7 November 2002*)

ABSTRACT: The alteration and transformation behaviour of montmorillonite (bentonite from Wyoming, MX-80) in low-salinity solutions (NaCl, $CaCl_2$) in the presence of metallic Fe (powder and $8 \times 4 \times 1$ mm plate) and magnetite powder was studied in batch experiments at 300°C to simulate the mineralogical and chemical reactions of clays in contact with steel in a nuclear waste repository. The evolutions of pH and solution concentrations were measured over a period of 9 months. The mineralogical and chemical evolution of the clays was studied by XRD, SEM, Transmission Mössbauer Spectroscopy and TEM (EDS, HR imaging and EELS). Dissolution of the di-octahedral smectite of the starting bentonite was observed, in favour of newly formed clays (chlorite and saponite), quartz, feldspars and zeolite. The formation of Fe-chlorite was triggered by contact with the metallic Fe plate and Fe-Mg-chlorite at distance from the Fe plate (>2 mm).

KEYWORDS: bentonite, smectite, Fe, magnetite, chlorite, saponite, experimental synthesis, EELS-TEM, EDS-TEM, HRTEM imaging, Mössbauer spectroscopy.

Bentonites are frequently recommended as backfill materials for the construction of high-level nuclear waste repositories. Different concepts foresee emplacing steel containers in tunnels backfilled with compacted bentonite (Madsen, 1998). Bentonites are choosen because of their swelling capacity, their low hydraulic conductivity when compacted to high density and their high sorption capacity. If the natural occurrence of old bentonites is an indication of their long-term stability, the very specific conditions of high-level nuclear wastes repository sites has to be taken into account, particularly the temperature increase and the eventual presence of available Fe. To this end, interactions between the bentonite and the container corrosion products are of particular interest. The key problem is the permanence or not of swelling minerals. Previous studies of the evolution of clay minerals in different natural contexts may provide part of the answer.

* E-mail: damien.guillaume@gr2.uhp-nancy.fr
† present address: Westfälische Wilhelms-Universität Münster, Institut für Mineralogie, Corrensstr. 24, 48149 Münster, Germany
DOI: 10.1180/0009855033830096

During diagenesis and low-temperature metamorphism of intermediate to mafic volcanic rocks and volcanogenic sediments, chlorite may crystallize from mineral precursors through complex processes including the crystallization of mixed-layer minerals (Bettison & Schiffman, 1988). Previous works suggest that precursors may be a smectite or other minerals such as berthierine (Aagaard *et al.*, 2000) which transform into chlorite in response to an increase of temperature (Hoffmann & Hower, 1979; Horton, 1985; Bettison & Schiffman, 1988; Schiffman & Fridleifsson, 1991; Humpreys *et al.*, 1994; Robinson & Santana de Zamora, 1999). The transition may occur in a stepped progression of smectite to chlorite via corrensite or as a gradual change involving randomly or regularly interlayered structures (chlorite-smectite: C-S), as dictated by the environment of formation (Bettison-Varga & Mackinnon, 1997). The role of fluid composition, porosity and water/rock ratio (W/R) in determining the stability of those minerals has been recognized. The role of low W/R ratio in the stabilization of C-S is emphasized (Alt *et al.*, 1986; Schiffman & Staudigel, 1995; Bettison-Varga & Mackinnon, 1997). Murakami *et al.* (1999) provided HRTEM evidence for the mechanism of the saponite-to-chlorite conversion in thermally metamorphosed volcanoclastic rocks and Robinson *et al.* (2002) gave a review of reaction pathways for the smectite-to-chlorite transformation in geothermal systems. However the complex structural and compositional changes that accompany the transformation are not entirely understood (Meunier *et al.*, 1991; Inoue & Utada, 1991), and the conditions favourable for the formation of chlorite have not been fully determined in most natural cases. Elementary thermodynamic considerations indicate that Fe-chlorite can only form when the Fe^{2+}/H^{+} ratio is high enough (Bowers *et al.*, 1984).

The smectite-to-chlorite transformation has not been reproduced experimentally. Small *et al.* (1992) indicated that no chlorite could be obtained experimentally under laboratory conditions below 400ºC, confirming previous statements from Gillery (1959) and Velde (1973). The hydrothermal stability of smectite has been studied extensively, especially the collapse of expandable smectite to non-expandable layer silicates, in particular illite, generally in mineral-solution systems devoid of added Fe (e.g. Eberl *et al.*, 1993; Cuadros & Linares, 1996; Mosser-Ruck *et al.*, 2001). In a number of studies, the formation of minor amounts of framework silicates after clay minerals was reported, but not studied in detail. The stability of smectite in the presence of Fe under low f_{O_2} is still poorly studied. Müller-Vonmoos *et al.* (1991) and Madsen (1998) studied the hydrothermal stability of bentonite in the presence of Fe and magnetite powders at 80ºC over a period of 27 to 29 weeks, but in a system free of liquid water. No mineralogical change was detected at this temperature. However, thermodynamic modelling (Cathelineau *et al.*, 2001) predicts a strong mineralogical evolution of the bentonite, especially the formation of a chlorite-saponite-zeolite assemblage, when the smectite-Fe system interacts with a solution at a temperature >150ºC.

In conclusion, the formation of chlorite is a possibility, established both from natural case studies and thermodynamic simulations. However, the availability of native Fe in contact with clay minerals in a high-level nuclear waste repository and its consequences for the evolution of clay minerals cannot be established from previous studies. Therefore, experiments have been performed to investigate the hydrothermal stability of a bentonite at 300ºC in the presence of metallic Fe and magnetite, and particularly the transformation of montmorillonite into Fe-rich clay phases, such as saponite and/or chlorite. Analytical investigations concerned both solid and liquid phases. Clay minerals were characterized by their structural (X-ray Diffraction – XRD, Scanning Electron Microscopy – SEM and High-Resolution Transmission Electron Microscopy – HRTEM imaging) and chemical properties (Cation Exchange Capacity – CEC, Transmission Mössbauer Spectroscopy – TMS, Electron Energy-Loss Spectroscopy – EELS and Energy Dispersive Spectroscopy (EDS)-TEM). The experimental solutions coexisting with the solid products were characterized by inductively coupled-atomic emission spectroscopy (ICP-AES) and inductively coupled plasma-mass spectroscopy (ICP-MS).

MATERIALS AND METHODS

Starting material

The MX80 bentonite (Na/Ca-bentonite, Wyoming), referred to as 'starting bentonite', was used for the experiments. Its CEC is 79 mEq/100 g (Table 1) and its composition is as follows

(Guillaume *et al.*, 2001a): montmorillonite (79%), quartz (3%), K-feldspar (2%), plagioclase (9%), carbonates (2%), mica (3%) and other minerals (mostly pyrite, phosphates and hematite, 2%). The structural formula of the montmorillonite (<2 μm fraction of the bentonite) determined from microprobe analyses, consistent with EDS-TEM and ICP-MS analyses, and taking into account the Fe^{2+}/Fe_{tot} ratio determined by TMS and EELS-TEM (Guillaume *et al.*, 2001b), is:

$$(Si_{3.98}Al_{0.02})(Al_{1.55}Mg_{0.28}Fe^{III}_{0.09}Fe^{II}_{0.08})O_{10}(OH)_2Na_{0.18}Ca_{0.10} \quad (1)$$

Preparation of the starting solid-solution system

The solution was prepared from analytical-grade chemicals. A Milli-Q Reagent Water System from Millipore Corp. provided deionized water with a resistivity >18 MΩ cm^{-1}. Na^+ and Ca^{2+} chlorides were added to deionized water to simulate the Na^+/Ca^{2+} ratio of natural water in sediments which is, in general, between 10 and 100. The starting solution contained 0.0207 mol/kg NaCl and 0.0038 mol/kg $CaCl_2$ and the total chloride concentration was 0.0282 mol/kg.

Bentonite (1.5 g) was first added to the solution with a liquid/solid mass ratio of 10, then metallic Fe and magnetite powders with an Fe/bentonite mass ratio of 0.1 (metallic Fe/magnetite: 1/1). Argon was bubbled through the preparation for 45 min to obtain an oxygen-free system and the preparation was equilibrated at room temperature for 6 days. The solution pH was then measured using a Mettler® combination pH electrode at 25ºC, and the Na^+/Ca^{2+} ratio of the reacting solution was ~80 (±2) as a result of exchange processes. Two types of assemblages, referred to as 'starting samples', were used: (1) bentonite with solution and addition of metallic Fe powder + magnetite powder; (2) the same with addition of an Fe plate with dimensions of 8 × 4 × 1 mm.

TABLE 1. Experimental conditions of the experiments and CEC (mEq/100 g) of the starting bentonite, starting sample, WIP and IP run samples.

Sample		CEC
	Starting bentonite	79
WIP		
25ºC	Starting sample	73
300ºC	3 months	75
	9 months	66
IP		
300ºC	1 week	n.a.
	1 month	n.a.
	3 months	73
	9 months	30

Experimental procedure

The experimental conditions are listed in Table 1. The starting samples were mounted under argon atmosphere in gold-lined warm-sealed great capacity autoclaves (~18 ml). The autoclaves were then heated to 300ºC in a furnace. The internal pressure, 86 bars, is the liquid-vapour equilibrium pressure at 300ºC. The durations of the experiments were 1 week, 1 month, 3 months and 9 months. The temperature control was stable to ~2ºC. The vessels were removed at specific time intervals, quenched at 25ºC and opened under argon atmosphere. Run samples were collected under argon atmosphere and centrifuged to extract the solution. Solution aliquots were taken, measured for pH and Eh and filtered through 0.45 then 0.02 μm filters into cleaned polypropylene bottles and analysed. When an Fe plate was added, the first 1 mm at the contact with the Fe plate was collected before centrifugation and analysed separately.

The solid was dried under argon flux at room temperature and gently ground in a mortar. Run samples were then stored in hermetically closed boxes under argon atmosphere until they were analysed. Solids were suspended again in pure water for the preparation of oriented samples for XRD, or in methanol for the preparation of TEM grids.

RESULTS

Three cases will be distinguished for the run samples formed: (1) at the nearest contact (<1 mm) with the Fe plate, denoted 'CIP run samples'; (2) at >1 mm from the Fe plate, denoted 'IP run samples'; and (3) during experiments performed without Fe plate, denoted 'WIP run samples'. In the CIP, IP and WIP cases, the same amounts of Fe and magnetite powders are present at the beginning of the experiment.

X-ray diffraction

The XRD data were collected with a D8 Bruker diffractometer with Co-$K\alpha_1$ radiation (λ = 1.7902 Å). The XRD patterns of unoriented powders were taken in duplicate to identify non-clay minerals. X-ray diffraction patterns were also taken from air-dried oriented and ethylene glycol (EG)-saturated specimens of the <2 μm fractions of the starting- and run samples.

The Greene-Kelly (Hoffman-Klemen) test was performed (Greene-Kelly, 1953; Hoffman & Klemen, 1950). The <2 μm fraction of each run sample was Li-saturated, heated overnight at 400ºC then glycerol saturated. Pure silica slides were used for oriented specimens of Li-saturated samples to avoid Na migration from the glass (Byström-Brusewitz, 1975).

Additional treatments included (1) K-saturation, heating overnight at 110ºC, heating then EG saturation, (2) Mg-saturation, then glycerol saturation, and (3) Li-saturation, then EG saturation.

Cation exchange capacity

The CEC values of the starting and run samples were determined as follows. Samples were Ba^{2+} saturated by treating them three times each with 1 N $BaCl_2$ solution, washed with distilled water and centrifuged until the electrical conductivity of the equilibrium solution was <10 μohm/cm^{-1}. The Ba^{2+} was then exchanged by treating the samples three times with 1 N $NaNO_3$ solution. The Ba^{2+} concentrations in the solutions were determined by atomic absorption spectrometry (AAS).

Scanning electron microscopy (SEM)

The SEM images were obtained using an Hitachi S-2500 Fevex scanning electron microscope. The denser fraction of each sample was separated by successive ultrasonication and sedimentation in alcohol, then disposed on carbon adhesives sticks. Semi-quantitative chemical analyses were also performed. The separated <2 μm fraction of each run-sample was also checked for newly formed non-clay minerals intimately associated with the clay.

Transmission Mössbauer spectroscopy (TMS)

^{57}Fe Mössbauer spectroscopy is the most proficient method to characterize the Fe species in solid phases. Mössbauer works on 'environmental' materials have been mainly concerned with Fe in two mineral groups: clay-sized phyllosilicates (often looked upon as clay minerals *sensu stricto*) and oxides. Ideally, a distinction of Fe in these two groups by Mössbauer spectroscopy is relatively straightforward: the phyllosilicates are paramagnetic at room temperature and may contain both divalent and trivalent Fe, whereas the most common Fe oxides should be magnetically ordered and contain only trivalent Fe, except for magnetite which is the only pure oxide of mixed valence (Murad, 1998).

Transmission Mössbauer spectra were collected using a constant-acceleration spectrometer with a 50 mCi source of ^{57}Co in Rh. The spectrometer was calibrated with a 25 μm foil of α-Fe at room temperature. Spectra were obtained at 12 K or 150 K. The cryostat consisted of a closed cycle helium Mössbauer cryogenic workstation with vibrations isolation stand manufactured by Cryo Industries of America. Helium exchange gas was used to thermally couple the sample to the refrigerator, allowing variable temperature operation from 12 to 300 K. The samples were set in the sample holder in a glove box filled with an Argon atmosphere and quickly transferred in the cryostat for Mössbauer measurements. Computer fittings were performed by using Lorentzian-shape lines. The parameters that result from any computer fitting must be both mathematically (χ^2 minimization) and physically significant; in particular the width of all lines must be small enough (Benali *et al.*, 2001).

Electron energy-loss spectroscopy (EELS)-transmission electron microscopy

The Fe^{3+}/Fe_{tot} ratio in isolated clay particles from the <2 μm fraction of the samples was determined using a Gatan® 666 parallel electron energy loss spectrometer attached to a CM20-Philips® instrument operating at 200 kV with an unsaturated LaB6 cathode. The following measuring conditions were chosen: a spectrometer entrance aperture of 2 mm, a collection half angle of 10 mrad, an energy dispersion of 0.2 eV per channel. The energy resolution, measured at the full width at half maximum (FWHM) of the zero-loss peak is 1.2 eV. Spectra were acquired at the thinnest part of the particles (<100 nm) and analysed with a Gatan® EL/P 2.1 PEELS software. The low energy-loss spectrum was used to remove the

multiple-ineslastic-scattering effect in the core-loss region using a Fourier-ratio deconvolution method (Egerton, 1986). Fitting of the Fe-L_3 edge was performed in the range 705 to 720 eV using Opus software® from Bruker and Fe^{3+}/Fe_{tot} ratio is determined using the method described by Guillaume *et al.* (2001b).

High-resolution transmission electron microscopy (HRTEM)

Selected samples were prepared for HRTEM using a JEOL JEM 2000 FX instrument operating at 200 kV. Preparation of the <2 µm fraction of samples for HR observations consisted of an

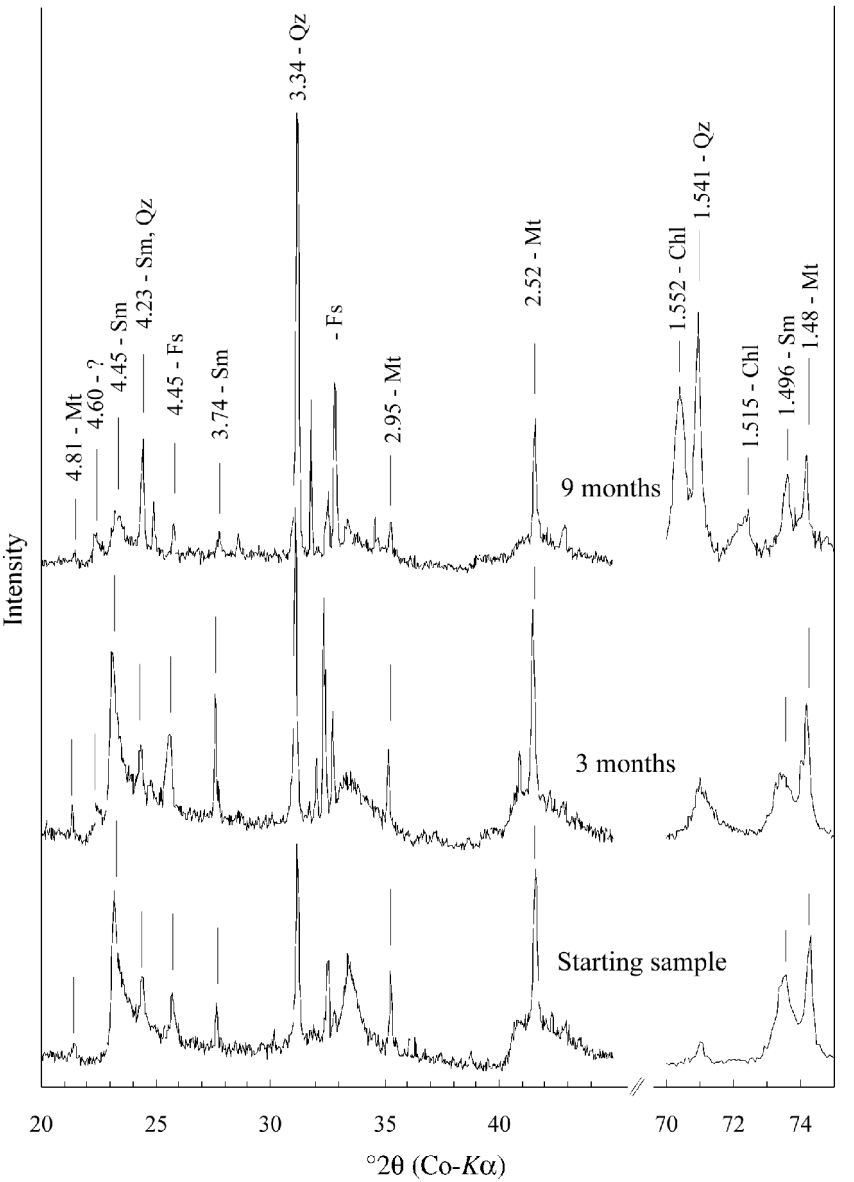

FIG. 1. XRD powder patterns of the starting sample, 3 month and 9 month IP run samples. Mt: magnetite; Sm: smectite; Qz: quartz; Fs: feldspar; Chl: chlorite. Reflection values in Å.

exchange with heptylamonium chloride (Lagaly *et al*., 1976), followed by an embedding in an Epon resin (Amouric & Olives, 1991). Ultrathin sections of the embedding blocks (100 nm) were prepared with an ultra-microtome equipped with a diamond knife, and transferred onto 300-mesh carbon-coated Ni grids.

Energy dispersive spectroscopy (EDS)

Microchemical analyses of isolated clay particles of the <2 μm fraction were obtained with an EDAX energy dispersive X-ray analyser attached to a CM20-Philips instrument operating at 200 kV equipped with Si-Li detector and Li super ultrathin windows SUTW. Spectra were collected under nanoprobe mode, over 40 s from an area ~10 nm in diameter. Elemental composition was calculated assuming the thin film criteria (SMTF program: semi-quantitative metallurgical thin film program) and using k-factors calibrated with independently analysed macroscopic micas, with a maximum error of 5% for each element. 30 to 50 analyses were performed on isolated particles for each sample. The structural formulae were calculated for each analysis taking into account the Fe^{3+}/Fe_{tot} ratio determined using EELS and TMS.

Analyses of run solutions

Chemical analyses of the experimental solutions were obtained by ICP-AES (Na^+, K^+, Ca^{2+}, Mg^{2+}, Fe^{2+} and Si^{4+} concentrations) and ICP-MS (Al^{3+} concentration). Solutions were acidified to avoid precipitation of Al or Fe hydroxides and diluted to bring concentrated analytes into quantification ranges of the ICP-AES and ICP-MS techniques. Because hydrochloric acid and sulphuric acid form poly-atomic species, nitric acid was chosen as the acidifying solution for both ICP-AES and ICP-MS analyses at 1.5% w/v and 3% w/v, respectively. The uncertainty in measured solution concentrations was ±10%.

Mineralogy of the Fe phases

XRD results. The Fe powder, which was added to the starting bentonite, was not detectable by XRD after 1 month of treatment and is not clearly observed with the SEM. In contrast to the Fe powder, no significant difference in the relative intensity of magnetite reflection lines was detected by XRD between the starting and run samples (Fig. 1), indicating that the amount of magnetite in the sample did not change significantly. However, the size of magnetite-like crystals observed with SEM is strongly modified. The starting magnetite powder was made of <5 μm grains (Fig. 2h). After 9 months, 40 to 200 μm euhedral crystals, of magnetite composition, are observed in the run samples (Fig. 2i).

TMS results. The TMS study (Fig. 3) also demonstrates the consumption of the metallic Fe powder. On the sides of the spectrum, one notices a magnetic component S (~7% of the total surface of the spectrum) ascribable to the maghemite (γ-$Fe^{III}{}_2O_3$, the oxidized form of magnetite). This indicates that magnetite is transformed to maghemite during the experiments.

Mineralogy of the non-clay phases

Observations by SEM are summarized in Table 2. Newly formed grains of quartz, K-feldspar, plagioclase and zeolites were observed in all run samples and overgrowths are observed on

TABLE 2. Assemblage of non-clay minerals in the starting bentonite (Guillaume *et al*., 2001a) and as observed by SEM in the starting sample, CIP and IP run samples.

Sample		Qz	Kfs	Plagio	Carb	Phos	Mica	Pyr	Sulph	Iron	Mt
Starting bentonite		3%	2%	9%	2%	+	3%	+	+		+
25ºC	Starting	+	+	+	+	+	+	+	+	+	+
300ºC	1 month	+	+	+		+	+			?	+
	3 months	+ Gr	+ Gr	+ Gr			+				+
	9 months	+ Gr	+ Gr	+ Gr			+				+

+: presence of the mineral; Gr: evidence for growing and neoformation; space: absence of the mineral. Kfs: K-feldspars, Plagio: plagioclase, Carb: carbonate, Phos: phosphate, Pyr: pyrite, Sulph: sulphate, Mt: magnetite

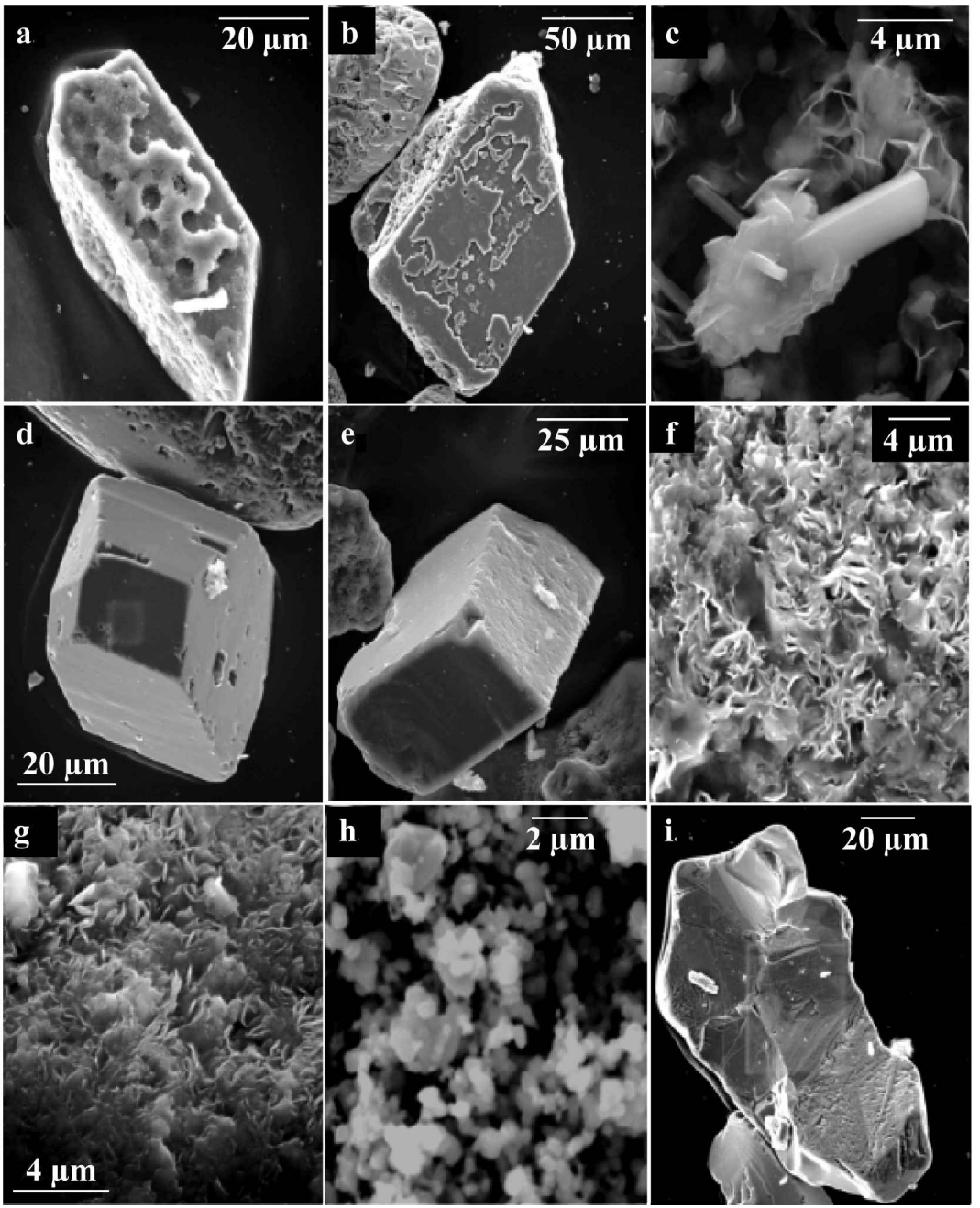

FIG. 2. Evolution of the morphology of primary minerals and newly formed minerals as seen by SEM: (a) growth of quartz on a quartz particle, (b) growth of K-feldspar on a plagioclase particle, (c) zeolite crystal associated with the clay, (d) newly formed plagioclase, (e) newly formed K-feldspar, (f) clay in the starting bentonite, (g) clay in the 3 month run sample, (h) magnetite powder added to the starting bentonite, (i) large euhedral crystal with magnetite composition. Micrographs a, g: 3 month WIP run sample; b, c, d, e, i: 9 month IP run sample.

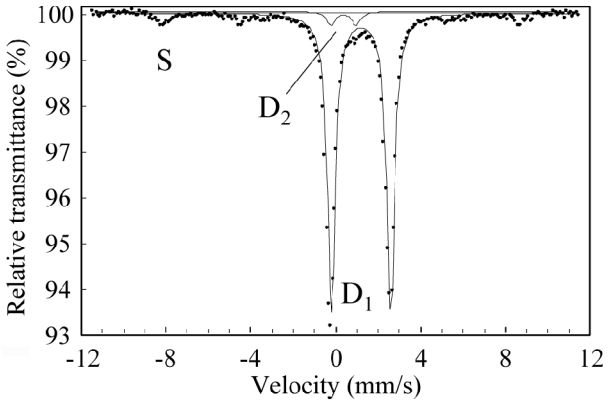

FIG. 3. TMS spectra of the 9 month IP run sample, measured at 11 K (see text for explanation of peak labels).

the anhedral detrital grains. Figures 2a and 2b show overgrowths of quartz grains and K-feldspar (microcline), respectively, on a plagioclase (albite) particle. Newly formed automorph particles of quartz, plagioclase (albite, Fig. 2d), and K-feldspar (microcline, Fig. 2e) were also observed. The XRD patterns of powder specimens of the 3 month and 9 month run samples (Fig. 1) show a strong increase in the 1.54 Å and 3.34 Å reflection (characteristic of quartz). This confirms that the amount of quartz is increasing.

No significant change was noticed in the morphology of the clay mass, as shown by Fig. 2f (clay fraction in the starting bentonite) and Fig. 2g (clay fraction in the 3 month run sample). Meanwhile, SEM observations showed fibrous particles of zeolites intimately associated with clay particles of the <2 μm fractions of 9 month IP and WIP run samples (Fig. 2c). Precise determination of the nature of these zeolite particles was not possible from semi-quantitative chemical analyses on SEM (mostly sodic with Si/Al ≈3.7, close to erionite composition). Based on XRD and SEM observations, zeolite was not present in the starting bentonite.

Mineralogy of the clay phase

XRD results - transformation of the montmorillonite in the absence of Fe plate (WIP run samples). Oriented slides were prepared for the starting sample and the 3 month and 9 month WIP run samples. The XRD patterns obtained before and after EG saturation are presented in Fig. 4. In air-dried specimens, with the duration of experiment we observe a strong decrease of the 12 Å peak (characteristic of the presence of a monovalent cation) and the increase of the 14.9 Å peak (characteristic of the presence of a divalent cation). This indicates that the sodi-calcic clay phase of the starting bentonite became progressively calcic, and is mostly calcic after 9 months. The 3 month run sample presents an intermediate state. The starting sample and the 3 month run sample both expand to ~17 Å after EG saturation, indicating that the clay phase is of smectite type. The 9 month sample expands to 16.8 Å, indicating that the clay phase is mostly of smectite type, and a small amount of mixed-layer clay might be present.

The Greene-Kelly test was performed on the same three samples. The XRD patterns obtained are presented in Fig. 5. The reflection around 9.5 Å for the starting sample indicates the presence of a montmorillonite. The strong reflection at 16.8 Å in the 9 month run sample indicates the presence of a tetrahedral charge deficiency. The 3 month run sample presents an intermediate state. This means that the montmorillonite progressively transforms to another mineral of the smectite group.

A starting-sample which is K-saturated, heated overnight at 110ºC, then EG saturated, expands to 16.9 Å (Fig. 6b) because of its low charge (0.38). After the same treatment, the 9 month run sample expands slightly to ~14 Å, indicating a high-charge smectite (Fig. 6c).

A 9 month run sample which is Mg saturated then glycerol saturated expands to 17 Å, however (Fig. 6d). This indicates that the clay phase of this sample is not of vermiculite type.

XRD results - evidence for a newly formed clay in experiments with added Fe plate (IP run samples). Additional peaks at 13.9 Å (weak),

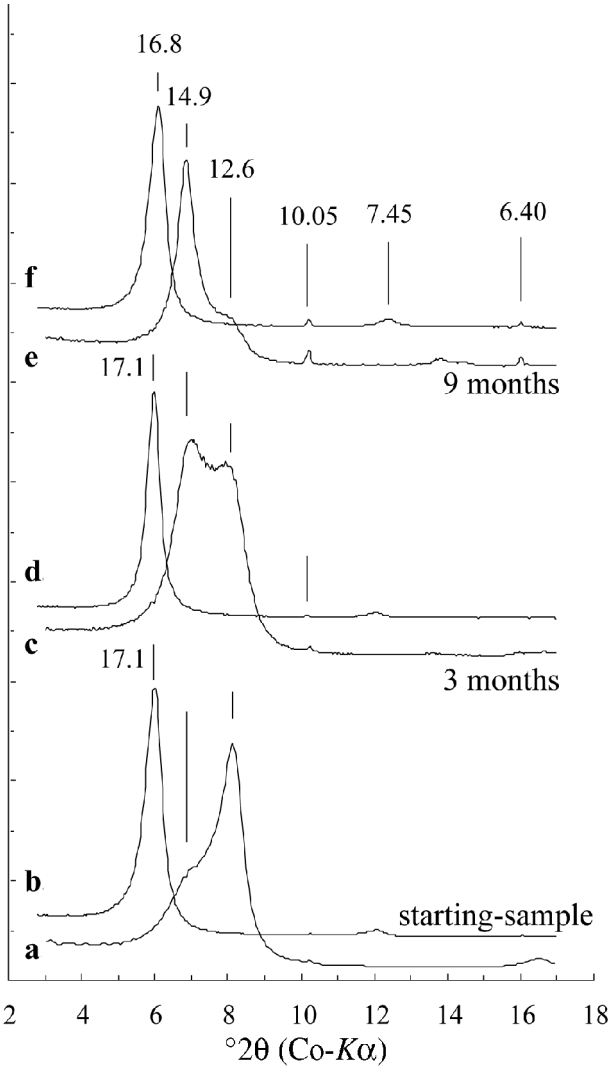

FIG. 4. XRD patterns of the starting sample, 3 month and 9 month WIP run samples. a, c, e: oriented, air-dried; b, d, f: EG-saturated. Reflection values in Å.

7.03 Å (strong) and 3.52 Å (medium) are present in the XRD pattern of the oriented Li-saturated 9 month IP run sample (Fig. 7a). The 13.9 Å reflection line is more clearly observed after heating the specimen at 330ºC, since Li-smectite formed a 'collapsed' structure (Fig. 7b). The above-mentioned additional peaks clearly indicate the presence of a mineral of the chlorite group. Heating the preparation at 550ºC modified the intensities of chlorite lines, diminishing the reflections of the second, third and fourth orders (Fig. 7c). The formation of an amorphous phase following the decomposition of chlorite at 550ºC can be observed in the range 30–33º2θ.

Chlorite does not expand by EG or glycerol saturation. On both EG- and glycerol-saturated XRD patterns of the 9 month run sample exchanged with Li and Mg, respectively, (Fig. 6e,f), reflections around 17 Å indicate the presence of smectite and shoulders around 14.4 Å indicate the presence of chlorite layers. Well-developed shoulders above 17 Å that are not present in the diffractogram of the starting sample are also observed (Fig. 6a). These shoulders indicate that a randomly inter-

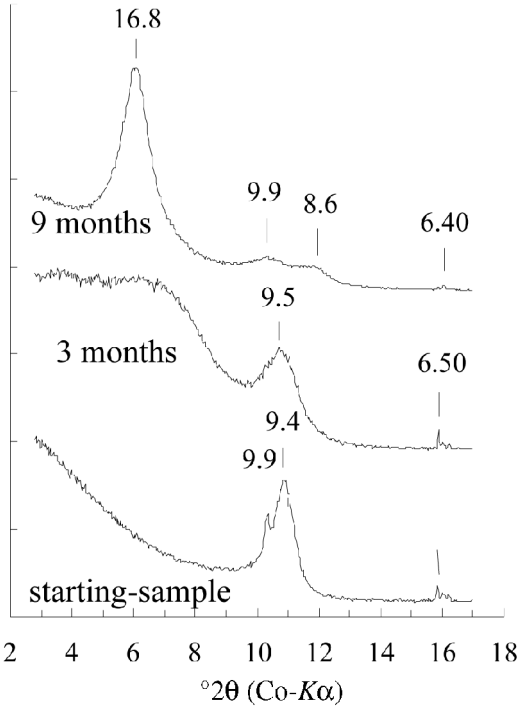

FIG. 5. XRD patterns of the starting sample, 3 month and 9 month WIP run samples, after the Greene-Kelly test. Reflection values in Å.

stratified chlorite-smectite structure is probably present in the 9 month run sample.

The XRD patterns of non-oriented powders of the 3 month and 9 month run samples in the range 70–75°2θ (Fig. 1), present two additional peaks at 1.515 Å and 1.552 Å which can be attributed to trioctahedral chlorite. The relative intensity of the 060 peak of dioctahedral smectite (d = 1.496 Å) decreased significantly and that of the 211 peak of quartz and/or the 060 peak of trioctahedral smectite (d = 1.541 Å) increased significantly.

The XRD data demonstrated that in the absence of added Fe plate (WIP run samples), montmorillonite progressively transforms to another clay of the beidellite–saponite–nontronite series. When an Fe plate is added to the experimental system (IP run samples), a chlorite-like mineral is also formed and the presence of a randomly interstratified clay is suspected.

CEC. The results of the CEC measurements for starting, IP and WIP run samples are summarized in Table 1. The CEC decreases with the duration of the treatment, and the decrease is very important when an Fe plate is added. This evolution can be attributed to strong mineralogical changes, such as the formation of non-expandable clay phases suggested by the XRD study.

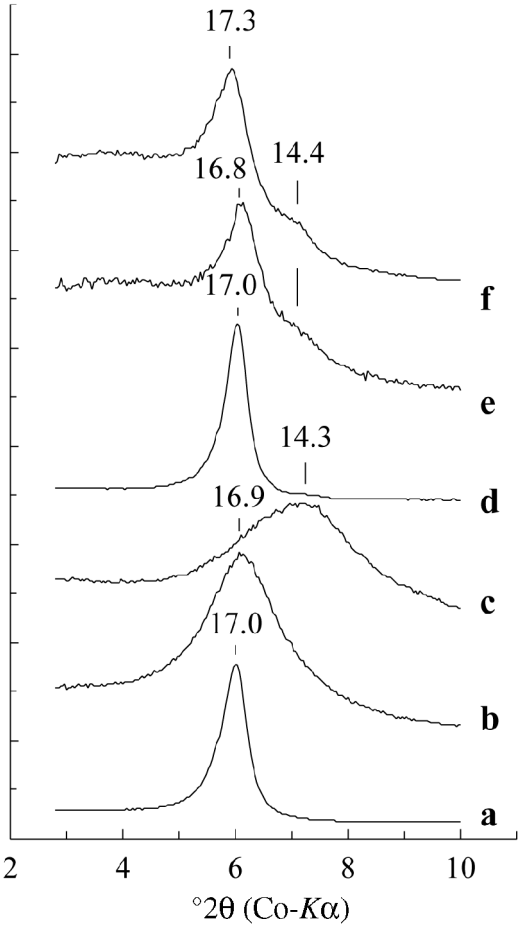

FIG. 6. XRD patterns of Li- K- and Mg-saturated samples. (a, b) starting sample, (a) Li- then EG-saturated, (b) K-saturated, 110°C heated then EG-saturated; (c, d) 9 months WIP run sample, (c) K-saturated, 110°C heated then EG-saturated, (d) Mg- then glycerol-saturated; (e, f) 9 month IP run sample, (e) Li- then EG-saturated, (f) Mg- then glycerol-saturated. Reflection values in Å.

HRTEM. High-resolution TEM observations of heptylammonium-saturated clay fractions (<2 μm) of the starting and 3 and 9 month IP run samples were performed to distinguish between different clay phases that might be present (low-charge smectite, saponite, vermiculite, chlorite, berthierine, etc.). According to Lagaly *et al.* (1976) and Vali & Hesse (1990), the difference between low-charge

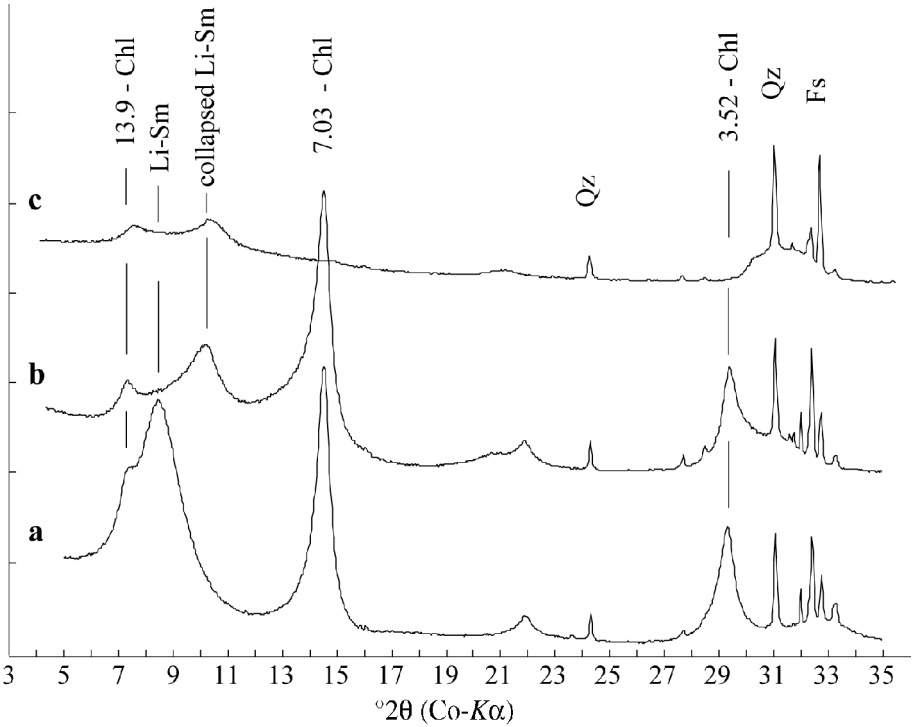

FIG. 7. XRD patterns of 9 month IP run sample. (a) Li-saturated, un-heated, (b) 330°C, (c) 550°C heated. Sm: smectite, Chl: chlorite, Qz: quartz, Fs: feldspars.

smectite (13 Å layer spacing), vermiculite and saponite (17–18 Å), chlorite (14 Å), and berthierine (7 Å) should be clearly observed. Figure 8a shows the layer structure of the montmorillonite in the starting-bentonite after treatment with heptylammonium ions, with layer spacing of ~13 Å. In the 3 month IP run sample, ~13 Å layers are still dominant, and some particles appear to be partly transformed to chlorite. Figure 8b shows the case of a particle presenting typical smectite layers (13 Å layer spacing) surrounded by three well identified chlorite layers (14 Å layer spacing). In the 9 month IP run sample, 14 Å layer spacing is dominant (Fig. 8c), but some particles are still not totally transformed and present some remaining layers with 13 Å spacing (Fig. 8d).

Neither 17–18 Å nor 7 Å layer spacing was observed, indicating that no saponite, vermiculite or berthierine were formed during the experiments. No regular interstratified smectite-chlorite particles were observed, indicating that the smectite-to-chlorite transition occurs via randomly interstratified particles.

Crystal-chemistry of the clay phase

The structural formulae of clay minerals are calculated from EDS analyses, taking into account the results obtained by EELS and TMS for the Fe^{3+}/Fe_{tot} ratio (see below). The clay particles were selected at random for EDS analysis. Consequently, the analytical points presented on the graphs do not necessarily represent the various populations (unreacted smectite, interstratified or newly formed particles). All structural formulae have been calculated on the basis of 11 and 14 oxygens as well as reference minerals because run samples are mixtures of di-octahedral smectite and tri-octahedral chlorite (mixed-layered minerals, or mechanical association of small-size particles). Following procedures already discussed in Schiffman & Fridleifsson (1991) for natural smectite–chlorite series, all figures show the totality of analytical data in diagrams calculated arbitrarily on a single basis (14 oxygens), since no quantitative parameters provide the relative amount of di-/trioctahedral phases in the studied run samples. All diagrams using structural formulae based on 11

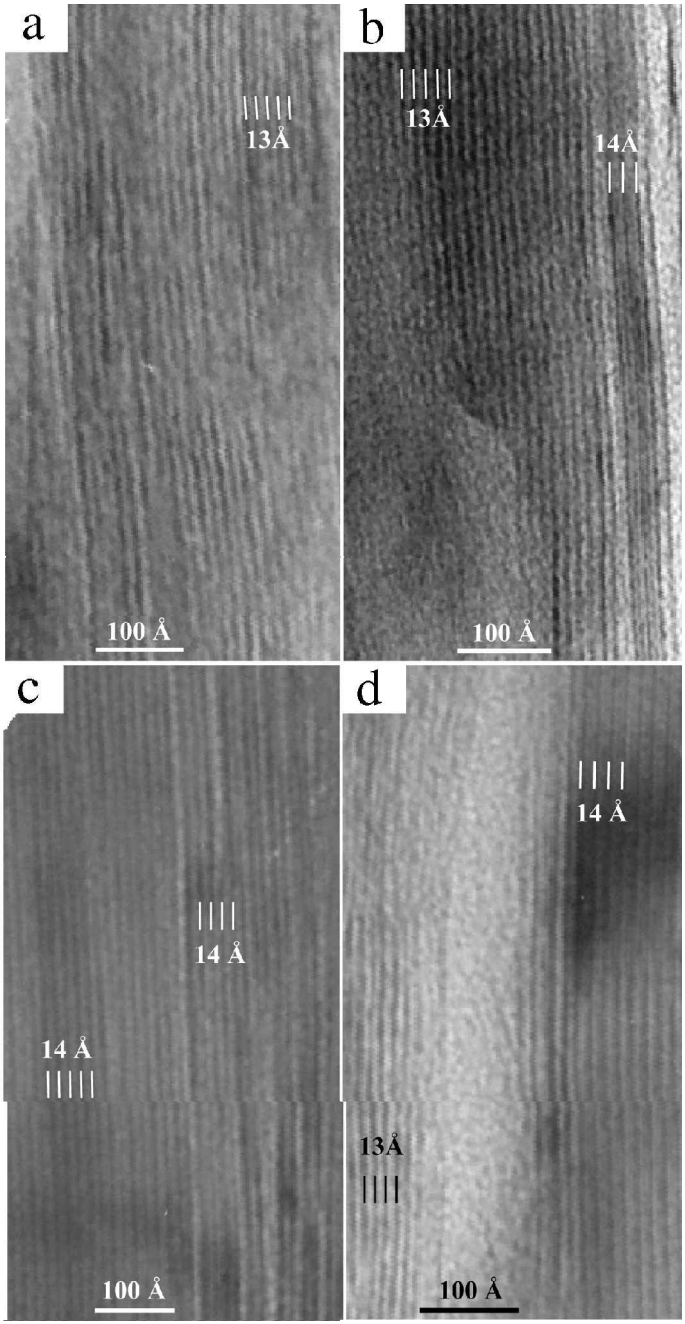

FIG. 8. HRTEM images of clay fractions from the starting sample (a), 6 month (b) and 9 month (c, d) IP run samples. Heptylamonium chloride-saturated specimens.

oxygens show, as expected, a similar distribution and relationships among analytical points and theoretical fields of reference minerals. Selected compositions (in wt.% of elements) of the 1 week, 1 month, 3 month and 9 month CIP, IP and WIP run samples are reported in Table 3.

Determination of the Fe^{3+}/Fe_{tot} ratio by TMS and EELS - TMS results. The spectrum obtained for the 9 month IP run sample (Fig. 3) shows a very strong paramagnetic component (doublet D1) corresponding to Fe^{II} characteristic of chlorite; ~90% of the total surface of the spectrum, indicating that Fe^{II} is fully incorporated into the clay. Another paramagnetic doublet (D2) in low abundance corresponding to Fe^{III} is also observed, indicating that Fe^{III} remains in the clay.

The Fe^{3+}/Fe_{tot} ratio in the clay fraction was calculated from Mössbauer spectra for the starting bentonite and the 3 and 9 month IP run samples. Results are reported as a function of time in Fig. 9a. In the montmorillonite of the starting-bentonite, the Fe^{3+}/Fe_{tot} ratio was of 0.55. We observe a strong evolution to a Fe^{3+}/Fe_{tot} ratio of 0.05 after 9 months, the 3 month run sample presenting an intermediate situation.

Determination of the Fe^{3+}/Fe_{tot} ratio by TMS and EELS - EELS results. The Fe^{3+}/Fe_{tot} ratio was also measured with EELS following the method published elsewhere (Guillaume *et al.*, 2001b) in isolated clay particles of the starting-bentonite (Guillaume *et al.*, 2001a) and clay fraction (<2 μm) of the 1 month, 3 month and 9 month CIP and IP run samples. Results are reported as a function of time in Fig. 9b. The overall evolution is consistent with TMS data, although EELS data show a larger dispersion which could be explained by the heterogeneity of the samples (see below). Deviation to higher Fe^{3+}/Fe_{tot} ratio could also be due to technical reasons such as sample preparation (that could not exclude selective sampling of particles) or sample oxidation under the beam.

For the 1 month, 3 and 9 month CIP and IP run samples, EELS and EDS analyses have been

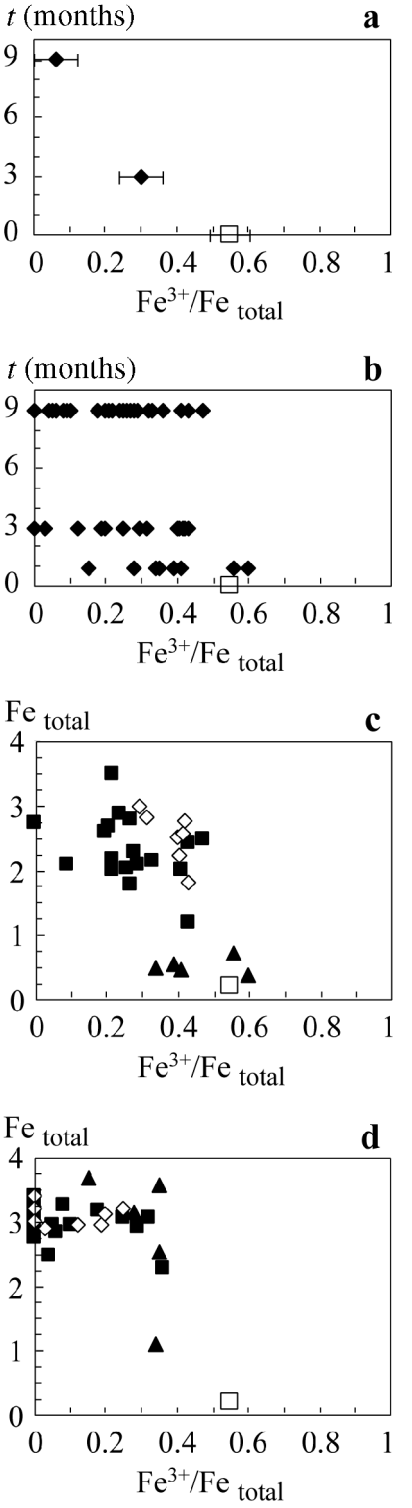

FIG. 9. Evolution of the Fe^{3+}/Fe_{tot} ratio, (a) in the clay phase of the IP run samples measured by TMS *vs.* experimental duration; (b) in isolated clay particles from CIP and IP run samples measured by EELS *vs.* experimental duration; (c and d) in isolated clay particles measured by EELS *vs.* iron content measured by EDS on the same particle (from structural formula calculated on the basis of 14 oxygens), (c) IP run samples, (d) CIP run samples. Filled triangles: 1 month; open diamonds: 3 months; filled squares: 9 month run samples. Comparison with the Fe^{3+}/Fe_{tot} ratio in the starting montmorillonite (open squares, Guillaume *et al.*, 2001b).

TABLE 3. Selected compositions (EDS analyses, in wt.% of elements) of CIP, IP and WIP run samples.

1 week CIP							1 week IP						
Si	Al	Fe	Mg	K	Na	Ca	Si	Al	Fe	Mg	K	Na	Ca
60.6	23.1	8.0	3.9	0.4	2.7	1.1	62.8	25.4	2.9	5.1	0.4	2.4	1.0
59.7	22.7	8.4	4.2	0.4	3.2	1.1	61.0	24.2	4.3	4.9	0.4	4.0	1.3
57.3	20.4	13.6	4.0	0.5	2.0	2.0	60.7	23.9	5.2	4.8	0.4	3.5	1.4
56.9	20.7	13.3	4.3	0.5	2.8	1.3	60.2	23.7	6.3	5.1	0.5	3.5	0.8
56.6	21.5	13.6	4.0	0.4	2.3	1.4	59.6	24.4	6.2	5.3	0.4	3.0	1.1
54.6	19.6	17.0	4.0	0.4	2.5	1.6	58.0	22.9	8.5	4.9	0.6	4.0	1.2
53.7	20.6	16.0	4.3	0.4	3.1	1.5	57.5	22.2	10.9	5.0	0.7	2.7	1.0
48.8	17.9	25.3	3.3	0.7	2.5	1.2	55.9	22.3	11.7	4.7	0.6	3.5	1.3
46.0	17.4	26.8	3.3	0.4	2.4	3.4	54.3	21.9	11.8	5.7	0.8	4.6	1.0
40.7	14.8	35.6	3.5	0.7	3.0	1.5	52.8	22.5	13.4	5.3	0.5	4.3	1.2

1 month CIP							1 month IP						
Si	Al	Fe	Mg	K	Na	Ca	Si	Al	Fe	Mg	K	Na	Ca
55.2	18.4	19.5	3.9	0.4	1.3	0.9	63.3	24.1	4.2	4.8	0.2	2.7	0.8
43.2	17.5	31.6	3.7	0.2	1.4	2.1	63.1	23.5	6.4	4.4	0.4	1.1	1.1
34.3	7.7	51.4	2.7	0.4	1.7	1.5	61.8	23.3	6.1	4.8	0.6	2.5	0.8
35.1	14.9	43.2	3.5	0.7	1.8	0.6	61.1	23.4	6.2	5.4	0.4	2.4	1.1
31.9	11.7	49.8	3.0	0.6	1.9	0.9	60.7	24.6	6.7	4.8	0.5	1.8	0.9
31.3	11.3	50.9	2.9	0.6	1.8	0.9	57.1	21.0	13.0	5.2	0.7	1.9	1.1
29.7	9.6	55.5	2.4	0.4	1.3	0.9	58.1	24.0	11.4	4.0	0.7	0.6	1.3
30.0	12.2	53.4	2.5	0.2	0.8	0.7	56.8	24.4	11.4	4.2	0.5	1.5	1.3
28.9	10.7	54.7	2.3	0.9	1.2	1.0	52.5	20.7	16.6	5.4	0.7	2.9	1.2
24.9	6.4	65.4	1.4	0.3	0.5	0.9	52.0	23.1	18.2	3.8	0.5	0.7	1.6

3 months CIP							3 months IP							3 months WIP						
Si	Al	Fe	Mg	K	Na	Ca	Si	Al	Fe	Mg	K	Na	Ca	Si	Al	Fe	Mg	K	Na	Ca
45.4	17.6	26.2	3.5	0.3	5.6	1.3	62.9	24.5	4.5	3.2	1.7	1.7	1.5	62	23	6.2	3.9	0.6	3.2	1.2
45.4	17.5	29.9	3.5	0.4	2.3	1.1	58.2	23.5	10.4	3.4	0.9	1.7	1.8	61	24	7.1	3.2	0.9	2.0	1.2
44.9	19.1	28.4	3.2	0.5	2.6	1.3	56.7	22.3	12.4	4.2	0.6	2.4	1.4	58	23	10	3.9	0.7	3.4	1.0
44.3	19.2	28.5	3.7	1.4	1.5	1.4	55.2	21.7	12.9	3.3	4.1	0.2	2.5	58	22	12	3.5	0.5	3.1	1.3
44.1	18.9	28.7	4.0	0.4	2.5	1.3	51.7	20.2	19.8	4.1	0.6	1.7	2.0	57	22	12	3.2	0.5	2.4	1.8
43.2	19.9	28.8	4.3	0.4	2.3	1.2	52.0	21.5	16.4	4.8	0.8	2.6	1.8	55	22	15	3.3	0.5	2.3	1.3
42.0	19.2	30.7	4.1	0.3	2.7	1.0	51.7	22.6	17.2	3.5	0.8	1.9	2.3	51	18	24	2.7	0.6	1.9	1.5
41.9	21.6	28.2	4.4	0.5	2.1	1.3	50.5	21.6	19.1	4.2	0.6	2.6	1.3	51	20	21	3.3	0.5	2.1	1.3
38.3	20.3	35.9	2.8	0.5	1.3	1.0	47.6	19.1	23.9	4.8	0.8	2.1	1.7	50	19	21	3.8	0.7	3.3	2.1
34.0	12.8	48.7	3.0	0.3	0.8	0.4	45.6	18.4	26.3	4.8	1.0	2.3	1.6	49	19	22	4.3	0.3	3.4	1.6

9 months CIP							9 months IP							9 months WIP						
Si	Al	Fe	Mg	K	Na	Ca	Si	Al	Fe	Mg	K	Na	Ca	Si	Al	Fe	Mg	K	Na	Ca
29.8	13.7	53.3	1.3	0.0	0.6	1.2	40.3	26.8	22.1	8.1	0.4	1.5	0.9	54	25	13	4	0.6	2.4	1.3
29.0	15.0	50.7	1.8	0.0	0.7	1.4	36.4	25.4	26.2	9.4	0.0	1.5	1.1	49	24	20	3.4	0.4	1.8	1.6
28.2	15.4	51.9	2.2	0.0	1.3	1.0	32.8	20.3	38.9	5.8	0.3	0.7	1.2	46	23	24	3.7	0.6	1.7	1.6
26.3	18.0	51.2	1.9	0.3	1.1	0.8	31.9	20.6	41.2	4.6	0.4	0.4	0.8	45	21	25	5	0.3	2.5	1.6
27.3	18.5	50.5	1.8	0.0	0.8	1.1	34.8	25.5	27.9	9.6	0.2	1.2	0.7	41	19	31	5.2	0.4	2.5	1.1
27.7	19.3	48.9	2.0	0.0	0.9	1.1	33.8	25.0	33.6	4.8	0.9	0.9	1.0	39	17	35	4.9	0.3	1.5	1.5
25.1	15.9	54.4	2.0	0.4	1.0	0.9	33.5	26.5	27.6	10.7	0.2	0.9	0.5	40	21	29	5.3	0.2	2.1	3.0
27.4	19.2	49.8	1.6	0.0	1.3	0.7	27.8	19.8	45.5	3.6	0.3	1.8	0.9	40	19	31	5.9	0.5	1.6	2.5
26.6	18.6	51.9	1.8	0.0	0.3	0.8	27.0	20.8	45.3	4.9	0.4	1.0	0.7	37	18	38	4.7	0.0	0.8	2.1
20.9	14.3	61.8	1.6	0.3	0.3	0.9	25.3	20.8	46.6	5.4	0.4	0.8	0.7							

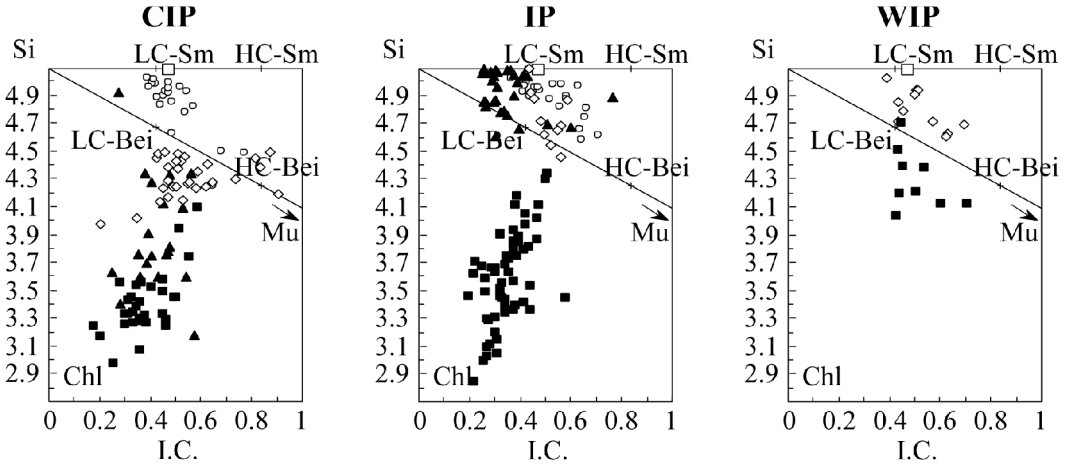

FIG. 10. Chemistry of the clay phase of the starting-sample (open square), 1 week (open circles), 1 month (filled triangles), 3 month (open diamonds) and 9 month (filled squares) CIP, IP and WIP run samples. Si *vs*. interlayer cations (I.C. = Na+2Ca+K), from structural formulae calculated on the basis of 14 oxygens. Reference minerals are reported: low-charge and high-charge smectite (LC-Sm, HC-Sm), low-charge and high-charge beidellite (LC-Bei, HC-Bei), muscovite (Mu), chlorite (Chl).

performed on the same particle in order to study the relationship between the Fe^{3+}/Fe_{tot} ratio and the Fe content of the clay phase. Results are reported in Fig. 9c and d. The Fe enrichment of the clay phase is well correlated with a decrease in the Fe^{3+}/Fe_{tot} ratio towards 0. This means that the newly formed clay mineral is mostly an Fe^{2+}-rich phase and intermediate compositions are due to partly transformed particles. This evolution is more efficient and rapid at the contact of the Fe plate.

Crystal-chemical changes of the run samples (EDS). The graphs presented in Figs 10 and 11 show a significant evolution in some cation site occupancies of the run products. The scatter of the analytical points for each run product indicates a chemical heterogeneity, which can be due to partly

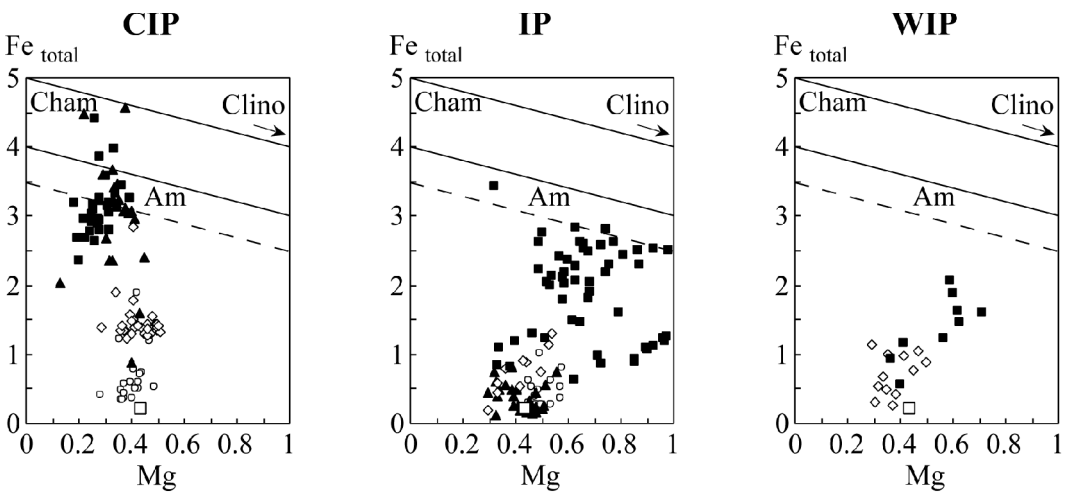

FIG. 11. Chemistry of the clay phase of the starting-sample (open square), 1 week (open circles), 1 month (filled triangles), 3 month (open diamonds) and 9 month (filled squares) CIP, IP and WIP run samples. Fe total *vs*. Mg, from structural formulae calculated on the basis of 14 oxygens. Reference minerals are reported: chamosite (Cham), clinochlore (Clino) and amesite (Am).

transformed particles or mechanical mixing of particles even at the smallest scale. The main changes in clay particle composition are the following.

Tetrahedral site: in both CIP and IP run samples, the Si content decreases drastically to a value of 2.9 for the longest experimental duration (Fig. 10). There is a continuous decrease in Si content for CIP run samples, at sub-constant interlayer charge first, and after 3 months, at decreasing interlayer charge down to a value of 0.2. The decrease in Si content is lower in IP than in CIP run samples for durations of 1 week to 3 months. However, the Si and interlayer charge are similar after 9 months in both CIP and IP run samples. In the case of WIP run samples, the transformation is different and the decrease in Si content only reaches a value of 4.1.

Octahedral site: in CIP run samples, a spectacular increase in the total Fe content is determined (Fig. 11). After 1 month, the CIP run sample contains 2.5 Fe and 3 to 3.5 after 9 months, with Fe contents up to 4.6 in some cases. In all CIP run samples, the Mg content remains sub-constant. For IP run samples, a similar increase in Fe content is noticed with time; however, the highest Fe content reaches a maximum value of 2.5 after 9 months, for a Mg content of 1, e.g. a value compatible with an Fe-for-Mg substitution at constant R^{2+} (±3.5). For WIP run samples, the same evolution as for IP is observed with Fe and Mg content only reaching the values of 2 and 0.6, respectively.

The overall evolution of the CIP, IP and WIP run samples is well discriminated in the diagram Fe/(Fe+Mg) *vs.* Si (Fig. 12). The discrimination of the two series of CIP and IP run samples is clear as a function of the Fe/Mg ratio, the duration of the experiment and the decrease of Si content (faster at the nearest contact with Fe plate). In the absence of added Fe plate (WIP run samples) the evolution is comparable to that of IP run sample.

The overall evolution of the clay (shown by the Si *vs.* interlayer cations (I.C.), Fig. 10) can be explained by two main changes in agreement with the preliminary interpretation of the TMS, EELS, CEC, HRTEM and XRD data; (1) a change in the nature of the expandable layers, with increasing tetrahedral charge, from montmorillonite to high-charge smectite; (2) the formation of chlorite. Mixing (or interstratification) between the starting montmorillonite and the high-charge smectite explains the first trend, then mixing (or inter-stratification) between smectite and chlorite explains the second trend. In the presence of a relatively large amount of Fe (presence of added Fe plate) these transformations are enhanced.

The high-charge smectite is a saponite, according to the compositional field in diagrams and the Fe^{3+}/Fe_{tot} ratio. Concerning the chlorite, crystal-chemistry shows a solid solution between an Fe-rich end-member and an Fe-Mg-rich chlorite depending on the distance from the added Fe plate. The recommended name for a ferrous-rich chlorite with such an Fe/Al content close to 2/1 is chamosite (Newman, 1987). The Fe-Mg chlorite belongs to the 'amesite' series, amesite, a 7 Å layer silicate, being used as a composition end-member only.

Solution chemistry

The solutions co-existing with the run samples were analysed when available. The results are summarized in Table 4. The pH measured after

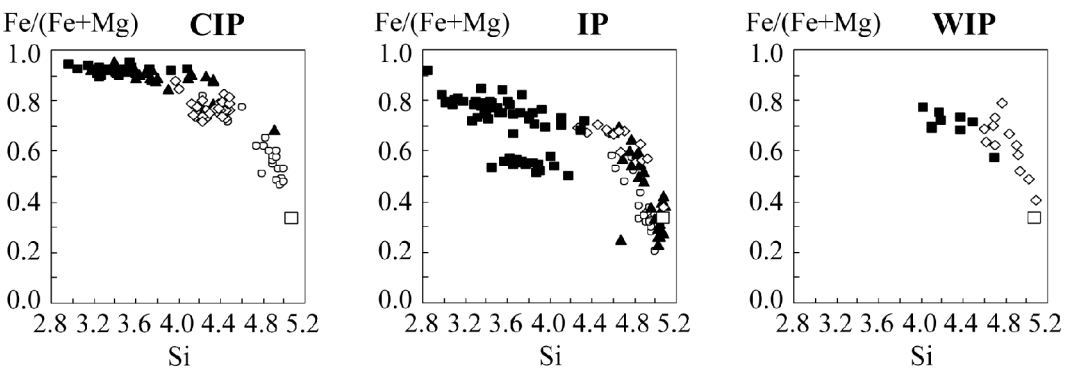

FIG. 12. Chemistry of the clay phase of the starting-sample (open square), 1 week (open circles), 1 month (filled triangles), 3 month (open diamonds) and 9 month (filled squares) CIP, IP and WIP run samples. Fe/(Fe+Mg) *vs.* Si, from structural formulae calculated on the basis of 14 oxygens.

TABLE 4. Chemistry of the initial solution, starting solution (after 6 days' equilibrium), WIP and IP run solutions.

Sample		pH	Eh (mV)	Si	Al	Fe	Mg	Ca	Na	K	Cl	Na/Ca
Initial solution		6.4	121	0	0	0	0	200	632	0	1032	5.5
WIP												
25ºC	Starting	7.2	−550	7	0	1	4	27	1272	18	1035	83
300ºC	3 months	5.5	−293	227	1	0	0	11	802	34	n.a.	131
	9 months	6.3	−157	76	1	0	1	15	876	55	1362	101
IP												
300ºC	1 day	n.a.	n.a.	486	36	17	9	25	908	82	1284	62
	1 week	n.a.	n.a.	410	10	5	6	22	762	96	1232	62
	1 month	6.5	−233	442	2	4	2	23	913	72	n.a.	69
	3 months	5.8	−260	265	1	2	1	9	762	35	n.a.	150

All concentrations in mg/l. n.a.: not analysed

cooling (at room temperature) and filtration of the experimental solution is presented as a function of the experiment duration in Fig. 13a. There is an initial decrease of run solution pH from 7.2 to 5.5, followed by an increase up to 6.3 for a duration of 9 months. Eh measured after cooling (at room temperature) and filtration of the experimental solution is ~−260 mV after 3 months and −213 mV after 9 months, i.e. significantly higher than in the starting solution (−550 mV) in the presence of metallic Fe (Fig. 13b). This might be due to a significant dissolution of metallic Fe and its passivation by magnetite or maghemite around the Fe plate.

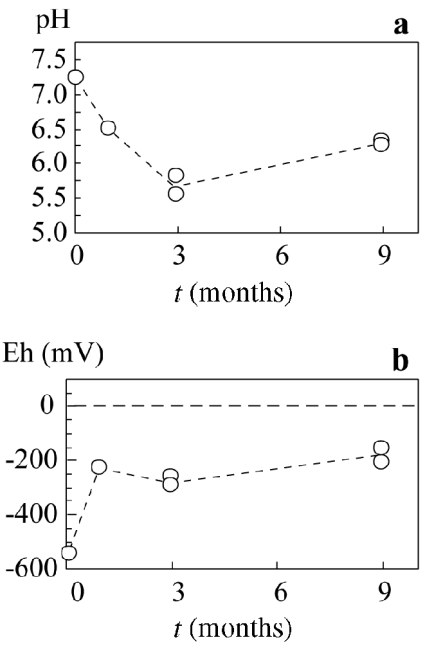

FIG. 13. Chemistry of run solutions. Evolution of pH (a) and Eh (b) *vs*. duration of experiments.

The evolution with time of the composition of the run solutions is reported in Fig. 14a–d. After 1 week of reaction with the bentonite at 300ºC, the Na^+/Ca^{2+} ratio of the reacting solution is ~60 (±2), but then increases up to values ranging from 100 to 150 depending on the experiments (Table 4). These changes in Na^+/Ca^{2+} are probably the result both of exchange processes, and uptake by framework silicates like feldspars and zeolites. The Cl^- content can be considered as sub-constant, and is not affected, as expected, by mineralogical changes.

The concentrations of Si, Al, Fe and Mg in the experimental solutions (Fig. 14a,b) display similar evolutions with time: a rapid increase during the first week and then a strong decrease for experiments of longer duration. The presence of Mg, Al and Fe in the solution during the first week suggests a partial dissolution of smectite and Fe-bearing phases.

Silicon is the most abundant element (except for Na and Cl initially present in the experimental solution). The Si concentration is high after 1 week (~500 mg/l, Fig. 14a). This result also suggests a rapid dissolution of several smectite layers. Then, the Si concentration decreases to ~250 mg/l (3 months), probably tending to values controlled by the equilibrium with quartz. Indeed, at 300ºC in moderately saline solution, Si saturation concentration (equilibrium with quartz) may be estimated at ~300–350 mg/l (Wolery, 1992; Wolery & Daveler, 1992). The value available for the longest experiment is much smaller. The Si content in the

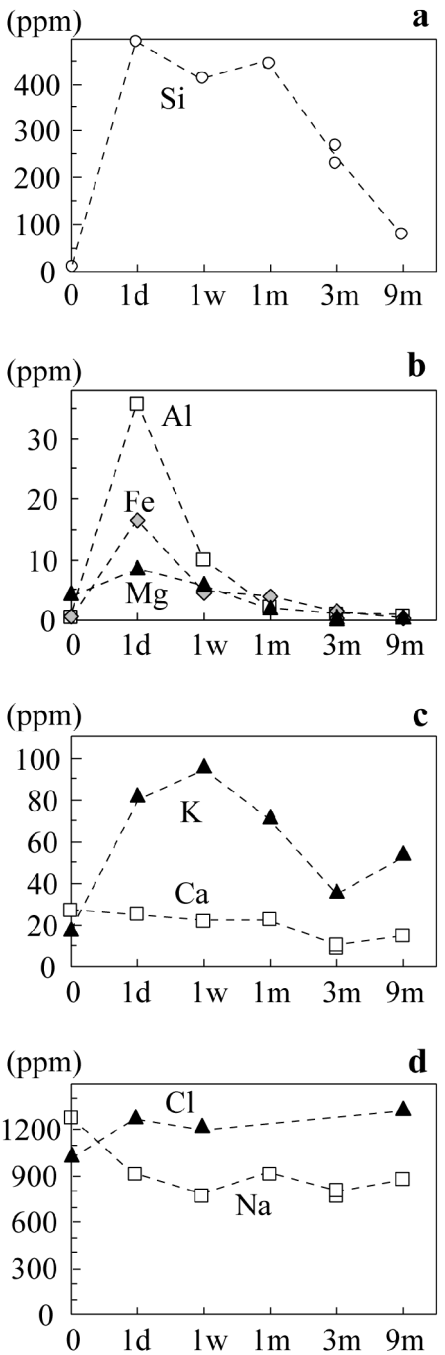

FIG. 14. Chemistry of run solutions. Evolution with time of the composition (ppm scale) for different cations; Si (a), Al, Fe and Mg (b), K and Ca (c), Na and Cl (d).

experimental solutions for the shortest duration explain why quartz crystallized in significant amounts. The analyses of the experimental solutions for experiments with the longest durations revealed very small Fe and Al concentrations. These elements are probably incorporated in the newly formed clays, zeolites and feldspars.

DISCUSSION

Evolution of Fe-bearing phases

The XRD and TMS data demonstrated that: (1) magnetite is transformed to maghemite and the total amount of magnetite-maghemite is stable; (2) the added Fe powder is rapidly consumed and, as the amount of magnetite-maghemite is stable, rapidly transformed to the soluble form (Fe^{2+}) during the experiment and/or incorporated into other minerals.

Newly formed non-clay minerals: quartz, feldspars and zeolite

The SEM and XRD data demonstrated the formation of newly formed quartz, felspars and zeolites. Other non-clay minerals that were present in the starting bentonite are rapidly consumed.

Silica is not fully incorporated within the newly formed clay minerals which are much poorer in silica than the montmorillonite of the starting bentonite. SiO_2 crystallizes as subeuhedral quartz. Equations written with constant Al and using the structural formulae of the starting- and run samples indicate that one mole Na/Ca-smectite may transform approximately into 0.91 moles of Fe-chlorite and 1.78 moles of quartz. The distribution of the silica released during the transformation of Si-rich minerals (smectite) into clay minerals with lower Si/Al ratios and quartz is difficult because at least two other types of silicates may crystallize, feldspars and zeolites. The occurence of such minerals as reaction products is consistent both with thermodynamic modelling predictions and data from other experiments on bentonites. Feldspars were commonly observed among reaction products in hydrothermal tests on Na- and K-montmorillonite between 260 and 400°C (Eberl & Hower 1977; Eberl 1978). Inoue (1983) reported the formation of Ca zeolites (wairakite and heulandite) as well as illite and smectite, from the reaction of Ca montmorillonite with 0.2 mol l^{-1} KOH at 300°C.

In addition, zeolites and feldspars associated with smectite and chlorite are commonly observed in alteration products of basic glasses of magmatic rocks submitted to hydrothermal alteration (among others, Cathelineau & Izquierdo, 1985; Cathelineau *et al.*, 1988; Schiffman & Fridleifsson, 1991).

Newly formed clay phases

Combined mineralogical and crystal-chemical studies of the run samples allowed us to understand and characterize the evolution of the clay minerals during the experiments. The XRD, CEC, TMS, EELS, EDS and HRTEM data demonstrated that hydrothermal treatment of the bentonite at 300ºC in the presence of Fe resulted in successive transformation of montmorillonite to saponite and trioctahedral chlorite (± randomly-interstratified chlorite-smectite).

The smectite-to-chlorite transformation occurred both via a dissolution-precipitation process and via a progressive, solid-state control, transformation of the particles. Partly transformed particles are detected by their intermediate compositions between the two end-members.

Comparison with natural systems

The final Fe mineral assemblage dominated by magnetite and the expected f_{O_2} is compatible with a natural reducing environment such as deep geothermal systems, or deep oceanic sediments. Therefore, the similarity between the newly formed mineral assemblages in natural systems and the experimental run products obtained in this study (chlorite, zeolites, quartz, saponite) might be emphasized.

A main difference in the run product described in the present experiments with many natural mineral assemblages is the scarcity of mixed-layered clays. The gradual or continuous transformation of smectite to chlorite, as accommodated through randomly interlayered C-S and regularly interlayered C-S (corrensite), is generally reported (Helmold & van de Kamp 1984; Chang *et al.* 1986; Bettison & Schiffman, 1988; Bevins *et al.* 1991). However, as already stated by Betisson-Varga & Mackinnon (1997), the decrease in smectite proportion is discontinuous as shown by the transition from smectite (with <20% chlorite) to corrensite and chlorite (with <10 % smectite) (Inoue *et al.*, 1984; Inoue, 1987; Inoue & Utada, 1991; Schiffman & Staudigel, 1995; Beaufort *et al.*, 1997). The main reason for such differences could be the experimental temperature (300ºC) sufficiently high to prevent the formation of berthierine or mixed-layered chlorite-smectite minerals. These minerals are considered to be stable only at lower temperatures: stability field of berthierine from 65 to 130ºC (Iijima & Matsumoto, 1982); from surface temperature to 100ºC (Velde *et al.*, 1975); C-S minerals formed between 200 and 240ºC (Schiffman & Fridleifsson, 1991).

In other cases, more complex mineral assemblages have been described, such as saponite-chlorite association as the ultimate product of alteration of beidellite (Schiffman & Fridleifsson, 1991). Such association is close to our experimental run products association.

CONCLUSIONS

Experiments at 300ºC in the presence of Fe powder and magnetite resulted in significant mineralogical changes, such as the formation of saponite, trioctahedral chlorite (±randomly-interstratified chlorite-smectite), quartz, feldspars and zeolite. The presence of the Fe plate in the system triggers reactions. Besides, Si, Al, Fe and Mg in the solution show a concomitant strong decrease in their concentrations, probably due to their incorporation in new silicates.

Concerning nuclear waste repositories, these experimental simulations demonstrated an evolution toward clay minerals having lower CEC. Meanwhile, this transformation is observed at the nearest contact with the added metallic Fe plate and under specific experimental conditions that are not representative of a nuclear wastes repository site where high temperature, and large amounts of water and Fe prevail.

This study also demonstrated the necessity of using complementary techniques operating at different scales for a complete understanding of the transformation that occurred during experiments.

ACKNOWLEDGMENTS

Experiments were conducted at the Géologie et Gestion des Ressources Minérales et Energétiques laboratory (G2R, CNRS-CREGU-INPL-UHP, Vandœuvre-lès-Nancy, France). The XRD data were collected at the Laboratoire Environnement et Minéralurgie (LEM,

CNRS-INPL, Vandœuvre-lès-Nancy, France), the SEM work was carried out at the Université Henri Poincaré (Vandœuvre-lès-Nancy, France), the TMS work at the Laboratoire de Chimie Physique et Microbiologie pour l'Environnement (LCPME, CNRS-UHP, Villers-lès-Nancy, France), the HRTEM imaging at the Centre de Recherche sur les Mécanismes de Croissance Cristalline (CRMC2, CNRS, National Facility for TEM/AEM, Marseilles, France), the EDS- and EELS-TEM work at the Université Henri Poincaré (Vandœuvre-lès-Nancy, France), and the ICP-AES and ICP-MS analyses of solutions at the Centre de Recherches Pétrographiques et Géochimiques (CRPG, CNRS, Vandœuvre-lès-Nancy, France).

The authors wish to thank J. Ghanbaja (UHP, Vandœuvre-lès-Nancy, France) for EELS and EDS analyses, I. Bihannic and F. Lhote (LEM, Vandœuvre-lès-Nancy, France) for their help and technical assistance with the XRD, and S. Nitsche (CRMC2, Marseilles, France) for HRTEM imaging. This research was supported financially by Andra – Agence Nationale pour la gestion des Déchets RadioActifs (French national agency for the management of radioactive wastes).

We thank L. Bettison-Varga, an anonymous reviewer and A. M. Karpoff, the Associate Editor, for their constructive comments.

REFERENCES

Aagaard P., Jahren J.S., Harstad A.O., Nilsen O. & Ramm M. (2000) Formation of grain-coating chlorite in sandstones. Laboratory synthesized *vs.* natural occurrences. *Clay Minerals*, 35, 261–269.

Alt J.C., Honnorez J., Laverne C. & Emmermann R. (1986) Hydrothermal alteration of 1 km section through the upper oceanic crust, DSDP Hole 504B: Mineralogy, chemistry and evolution of seawater-basalt interaction. *Journal of Geophysical Research*, **91**, 10309–10335.

Amouric M. & Olives J. (1991) Illitization of smectite as seen by high-resolution transmission electron microscopy. *European Journal of Mineralogy*, **3**, 831–835.

Beaufort D., Baronnet A., Lanson B. & Meunier A. (1997) Corrensite: a single phase or a mixed layered phyllosilicate of the saponite-clorite conversion series? The case study of the Sancerre-Couy deep drill-hole (France). *American Mineralogist*, **82**, 109–124.

Benali O., Abdelmoula M., Refait P. & Génin J.M. (2001) Effect of orthophosphate on the oxidation products of Fe(II)-Fe(III) hydroxycarbonate: the transformation of green rust to ferrihydrite. *Geochimica et Cosmochimica Acta*, **65**, 1715–1726.

Bettison L. & Schiffman P. (1988) Compositional and structural variations of phyllosilicates from the Point Sal ophiolite, California. *American Mineralogist*, **73**, 62–76.

Bettison-Varga L. & Mackinnon I.D.R. (1997) The role of randomly mixed-layered chlorite/smectite in the transformation of smectite to chlorite. *Clays and Clay Minerals*, **45**, 506–516.

Bevins R.E., Robinson D. & Rowbotham G. (1991) Compositional variations in mafic phyllosilicates from regional low-grade metabasites and application of the chlorite geothermometer. *Journal of Metamorphic Geology*, **9**, 711–721.

Bowers T.S., Jackson K.J. & Helgeson H.C. (1984) *Equilibrium Activity Diagrams for Coexisting Minerals and Aqueous Solutions at Pressures and Temperatures to 5 kb and 600ºC*. Springer-Verlag, Berlin.

Byström-Brusewitz A.M. (1975) Studies of the Li test to distinguish beidellite and montmorillonite. *Proceedings of the International Clay Conference, Mexico City*, pp. Pp. 419–428, Applied Publishing Ltd., Wilmette, Illinois, USA.

Cathelineau M. & Izquierdo G. (1988) Temperature-composition relationships of authigenic micaceous minerals in the Los Azufres geothermal system. *Contributions to Mineralogy and Petrology*, **100**, 418–428.

Cathelineau M., Oliver R., Nieva D. & Garfias A. (1985) Mineralogy and distribution of hydrothermal mineral zones in Los Azufres (Mexico) geothermal field. *Geothermics*, **14**, 49–57.

Cathelineau M., Mosser-Ruck R. & Charpentier D. (2001) Interactions fluides/argilites en conditions de stockage profond des déchets nucléaires. Intérêt du couplage expérimentation/modélisation dans la compréhension des mécanismes de transformation des argiles et la prédiction à long terme du comportement de la barrière argileuse. Pp. 305–341 in: *Actes des Journées Scientifiques ANDRA*, EDP Sciences Nancy, France.

Chang H.K., Mackenzie F.T. & Schoonmaker J. (1986) Comparison between the diagenesis of dioctahedral and trioctahedral smectite, Brasilian offshore basins. *Clays and Clay Minerals*, **34**, 407–423.

Cuadros J. & Linares J. (1996) Experimental kinetic study of the smectite-to-illite transformation. *Geochimica et Cosmochimica Acta*, **60**, 439–453.

Eberl D. (1978) Series for dioctahedral smectites. *Clays and Clay Minerals*, **26**, 327–340.

Eberl D. & Hower J. (1977) The hydrothermal transformation of sodium and potassium smectite into mixed-layer clay. *Clays and Clay Minerals*, **25**, 215–227.

Eberl D., Velde B. & McCormick T. (1993) Synthesis of illite-smectite from smectite at earth surface temperatures and high pH. *Clay Minerals*, **28**, 49–60.

Egerton R.F. (1986) *Electron Energy-loss Spectroscopy*

in the Electron Microscope. Plenum, New York.

Gillery F.H. (1959) The X-ray study of synthetic Mg-Al serpentines and chlorites. *American Mineralogist*, **44**, 143–152.

Greene-Kelly R. (1953) The identification of montmorillonoids in clays. *Journal of Soil Science*, **4**, 233–237.

Guillaume D., Neaman A., Mosser-Ruck R., Dubessy J., Cathelineau M. & Villiéras F. (2001a) Experimental study of hydrothermal reactivity of bentonite at 80 and 300ºC in the presence of iron and/or iron oxides. *Berichte der Deutschen Mineralogischen Gesellshaft, Beihefte zum European Journal of Mineralogy*, **13**, 69 pp.

Guillaume D., Pironon J. & Ghanbaja J. (2001b) Valence determination of iron in clays by electron energy loss spectroscopy. *Berichte der Deutschen Mineralogischen Gesellshaft, Beihefte zum European Journal of Mineralogy*, **13**, 70 pp.

Helmold K.P. & van de Kamp P.C. (1984) Diagenetic mineralogy and controls on albitization and laumontite formation in Paleogene arkoses, Santa Ynez Mountains, California. Pp. 239–276 in: *Clastic Diagenesis* (D.D. McDonald & R.C. Surdam, editors). American Association of Petroleum Geologists Memoir **37**.

Hoffman U. & Klemen E. (1950) Loss of exchangeability of lithium ions in bentonites on heating. *Zeitschrift für Anorganische und Allgemeine Chemie*, **262**, 95–99.

Hoffmann J. & Hower J. (1979) Clay mineral assemblages as low grade metamorphic geothermometers: Application to the thrust-faulted disturbed belt of Montana, USA. *Society of Economic Paleontologists and Mineralogists Special Publication*, **26**, 55–79.

Horton D.G. (1985) Mixed-layer illite/smectite as a paleotemperature indicator in the Amethyst vein system, Creed district, Colorado, USA. *Contributions to Mineralogy and Petrology*, **91**, 171–179.

Humphreys B., Kemp S.J., Lott G.K., Bermanto Dharmayanti D.A. & Samsori I. (1994) Origin of grain-coating chlorite by smectite transformation: an example from Miocene sandstones, North Sumatra Back-Arc Basin, Indonesia. *Clay Minerals*, **29**, 681–692.

Iijima A. & Matsumoto R. (1982) Berthierine and chamosite in coal measures of Japan. *Clays and Clay Minerals*, **30**, 264–274.

Inoue A. (1983) Potassium fixation by clay minerals during hydrothermal treatment. *Clays and Clay Minerals*, **31**, 81–91.

Inoue A. (1987) Conversion of smectite to chlorite by hydrothermal diagenetic alterations, Hokuroku Kuroko mineralization area, Northeast Japan. *Proceedings of the International Clay Conference, Denver*, pp. 158–164. The Clay Minerals Society, Bloomington, Indiana, USA.

Inoue A. & Utada M. (1991) Smectite-to-chlorite transformation in thermally metamorphosed volcanoclastic rocks in the Kamikita area, North Honshu, Japan. *American Mineralogist*, **76**, 628–640.

Inoue A., Utada M., Nagata H. & Watanabe T. (1984) Conversion of trioctahedral smectite to interstratified chlorite/smectite in Pliocene acidic pyroclastic sediments of the Ohyu district, Akita Prefecture, Japan. *Clay Science*, **6**, 103–106.

Lagaly G., Fernandez Gonzalez M. & Weiss A. (1976) Problems in layer-charge determination of montmorillonites. *Clay Minerals*, **11**, 173–187.

Madsen F.T. (1998) Clay mineralogical investigations related to nuclear waste disposal. *Clay Minerals*, **33**, 109–129.

Meunier A., Inoue A. & Beaufort D. (1991) Chemiographic analysis of trioctahedral smectite-to-chlorite conversion series from the Ohyu Caldera, Japan. *Clays and Clay Minerals*, **39**, 409–415.

Mosser-Ruck R., Pironon J., Cathelineau M. & Trouiller A. (2001) Experimental illitization of smectite in a K-rich solution. *European Journal of Mineralogy*, **13**, 829–840.

Müller-Vonmoos M., Kahr G., Bucher F., Madsen F.T. & Mayor P.A. (1991) *Untersuchungen zum Verhalten von Bentonit in kontakt mit Magnetit und Eisen unter Endlagerbedingungen*. NTB 91-14. Nagra, Hardstrasse 73, CH-5430 Wettingen, Switzerland.

Murad E. (1998) Clays and clay minerals: What can Mössbauer spectroscopy do to help understand them? *Hyperfine Interactions*, **117**, 39–70.

Murakami T., Sato T. & Inoue A. (1999) HRTEM evidence for the process and mechanism of saponite-to-chlorite conversion through corrensite. *American Mineralogist*, **84**, 1080–1087.

Newman A.C.D., editor (1987) *Chemistry of Clays and Clay Minerals*. Monograph **6**. Mineralogical Society, London.

Robinson D. & Santana de Zamora A. (1999) The smectite to chlorite transition in the Chipilapa geothermal system, El Salvador. *American Mineralogist*, **78**, 607–619.

Robinson D., Schmidt S.Th. & Santana de Zamora A. (2002) Reaction pathways and reaction progress for the smectite-to-chlorite transformation: evidence from hydrothermally altered metabasites. *Journal of Metamorphic Geology*, **20**, 167–174.

Schiffman P. & Fridleifsson G.O. (1991) The smectite-chlorite transition in drillhole Nj-15, Nesjavellir geothermal field, Iceland: XRD, BSE, and Electron Microprobe Investigations. *Journal of Metamorphic Geology*, **9**, 679–696.

Schiffman P. & Staudigel H. (1995) The smectite to chlorite transition in a fossil seamount hydrothermal system: the basement complex of La Palma, Canary

Islands. *Journal of Metamorphic Geology*, **13**, 487–498.

Small J.S., Hamilton D.L. & Habesch S. (1992) Experimental simulation of clay precipitation within reservoir sandstones 1: Techniques and examples. *Journal of Sedimentary Petrology*, **62**, 508–519.

Vali H. & Hesse R. (1990) Alkylammonium ion treatment of clay minerals in ultrathin section: A new method for HRTEM examination of expandable layers. *American Mineralogist*, **75**, 1443–1446.

Velde B. (1973) Phase equilibria studies in the system MgO-AlO-SiO-UO: chlorite and associated minerals. *Mineralogical Magazine*, **39**, 297–312.

Velde B., Raoult J.-F. & Leikine M. (1975) Metamorphosed berthierine pellets in mid-Cretaceous rocks from northeastern Algeria. *Journal of Sedimentary Petrology*, **39**, 1275–1280.

Wolery T.J. (1992) *EQ3NR, a computer program for geochemical aqueous speciation solubility calculations: theoretical manual, user's guide and related documentation* (Version 7.0). UCRL-MA-110662-PT-III, Laurence Livermore National Laboratory, Livermore, California.

Wolery T.J. & Daveler S.A. (1992) *EQ6, a computer program for reaction path modeling of aqueous geochemical systems: theoretical manual, user's guide and related documentation* (Version 7.0). UCRL-MA-110662-PT-IV, Laurence Livermore National Laboratory, Livermore, California.